NASA/CR-2007-214858

CFD Analysis of Tile-Repair Augers for the Shuttle Orbiter Re-Entry Aeroheating

Ali R. Mazaheri
Analytical Mechanics Associates, Inc., Hampton, Virginia

April 2007

The NASA STI Program Office . . . in Profile

Since its founding, NASA has been dedicated to the advancement of aeronautics and space science. The NASA Scientific and Technical Information (STI) Program Office plays a key part in helping NASA maintain this important role.

The NASA STI Program Office is operated by Langley Research Center, the lead center for NASA's scientific and technical information. The NASA STI Program Office provides access to the NASA STI Database, the largest collection of aeronautical and space science STI in the world. The Program Office is also NASA's institutional mechanism for disseminating the results of its research and development activities. These results are published by NASA in the NASA STI Report Series, which includes the following report types:

- TECHNICAL PUBLICATION. Reports of completed research or a major significant phase of research that present the results of NASA programs and include extensive data or theoretical analysis. Includes compilations of significant scientific and technical data and information deemed to be of continuing reference value. NASA counterpart of peer-reviewed formal professional papers, but having less stringent limitations on manuscript length and extent of graphic presentations.

- TECHNICAL MEMORANDUM. Scientific and technical findings that are preliminary or of specialized interest, e.g., quick release reports, working papers, and bibliographies that contain minimal annotation. Does not contain extensive analysis.

- CONTRACTOR REPORT. Scientific and technical findings by NASA-sponsored contractors and grantees.

- CONFERENCE PUBLICATION. Collected papers from scientific and technical conferences, symposia, seminars, or other meetings sponsored or co-sponsored by NASA.

- SPECIAL PUBLICATION. Scientific, technical, or historical information from NASA programs, projects, and missions, often concerned with subjects having substantial public interest.

- TECHNICAL TRANSLATION. English-language translations of foreign scientific and technical material pertinent to NASA's mission.

Specialized services that complement the STI Program Office's diverse offerings include creating custom thesauri, building customized databases, organizing and publishing research results ... even providing videos.

For more information about the NASA STI Program Office, see the following:

- Access the NASA STI Program Home Page at ***http://www.sti.nasa.gov***

- E-mail your question via the Internet to help@sti.nasa.gov

- Fax your question to the NASA STI Help Desk at (301) 621-0134

- Phone the NASA STI Help Desk at (301) 621-0390

- Write to:
  NASA STI Help Desk
  NASA Center for AeroSpace Information
  7115 Standard Drive
  Hanover, MD 21076-1320

NASA/CR-2007-214858

CFD Analysis of Tile-Repair Augers for the Shuttle Orbiter Re-Entry Aeroheating

Ali R. Mazaheri
Analytical Mechanics Associates, Inc., Hampton, Virginia

National Aeronautics and
Space Administration

Langley Research Center
Hampton, Virginia 23681-2199

Prepared for Langley Research Center
under Grant NNL06AC49T

April 2007

Available from:

NASA Center for AeroSpace Information (CASI)
7115 Standard Drive
Hanover, MD 21076-1320
(301) 621-0390

National Technical Information Service (NTIS)
5285 Port Royal Road
Springfield, VA 22161-2171
(703) 605-6000

Abstract

A three-dimensional aerothermodynamic model of the shuttle orbiter's tile overlay repair (TOR) sub-assembly is presented. This sub-assembly, which is an overlay that covers the damaged tiles, is modeled as a protuberance with a constant thickness. The washers and augers that serve as the overlay fasteners are modeled as cylindrical protuberances with constant thicknesses. Entry aerothermodynamic cases are studied to provide necessary inputs for future thermal analyses and to support the space-shuttle return-to-flight effort. The NASA Langley Aerothermodynamic Upwind Relaxation Algorithm (LAURA) is used to calculate heat transfer rate on the surfaces of the tile overlay repair and augers. Gas flow is modeled as non-equilibrium, five species air in thermal equilibrium. Heat transfer rate and surface temperatures are analyzed and studied for a shuttle orbiter trajectory point at Mach 17.85. Computational results show that the average heat transfer rate normalized with respect to its value at body point 1800 is about BF=1.9 for the auger head. It is also shown that the average BF for the auger and washer heads is about BF=2.0.

Nomenclature

(i, j, k)	Grid points indices in curvilinear computational coordinates
(x, y, z)	Reference coordinate system
α	Angle of attack
δ	Boundary layer thickness
ϵ	Emissivity
d	Protuberance diameter
d	Spacer diameter
d_{auger}	Auger head diameter
H	Altitude
h	Spacer height
k	Tile overlay thickness
M	Mach number
T	Temperature
U	Velocity
BF	Normalized heat transfer rate, Bump Factor
BPt	Body Point
CAIB	*Columbia* Accident Investigation Board
ISS-HVFW	International Space Station Heavy Vehicle Forward Weight
LAURA	Langley Aerothermodynamic Upwind Relaxation Algorithm
RCG	Reaction Cured Glass
RTF	Return to Flight
SiC	Silicon Carbide
STS	Space Transportation System
TOR	Tile Overlay Repair
TPS	Thermal Protection System

1 Introduction

This report, prepared at the request of the Orbiter Tile Overlay Repair project, represents a formal delivery of analysis results from NASA Langley Research Center to Johnson Space Center.

A description of the process utilized to perform Orbiter tile damage assessment is reported by Campbell et al. [2]. In that report, individual aeroheating tools with nominal re-entry heating environment characterizations are emphasized, where Orbiter aeroheating environment is defined by nominal smooth body heating. *Smooth body* refers to an undamaged Thermal Protection System (TPS). Accordingly, critical damage to the TPS is characterized by three different damage scenarios. These scenarios are damage that 1) does not generate a catastrophic situation but may create a sequence of significant damage propagations which leads to an unsafe situation, 2) does not generate a catastrophic situation but minimal damage propagation may lead to an unsafe situation, 3) does generate an unsafe situation due to a severe damage. In this report, only the tile damage that is considered as a second category problem out of these scenarios is addressed. The current tile-repair option is a thin shell outer surface barrier, which is referred to as the Tile Overlay. This tile overlay is a thin Carbon Silicon Carbide plate that is being placed on a damaged surface of the orbiter and attached with several screws and washers. These screws and washers are known as augers and spacers, respectively. Figure (1) shows the tile overlay, cavity insulation, gasket, and fasteners. Aerothermodynamic analyses of the tile overlay repair are reported by Lessard [7]. In his study, effects of the overlay fasteners on surface heat fluxes were not included.

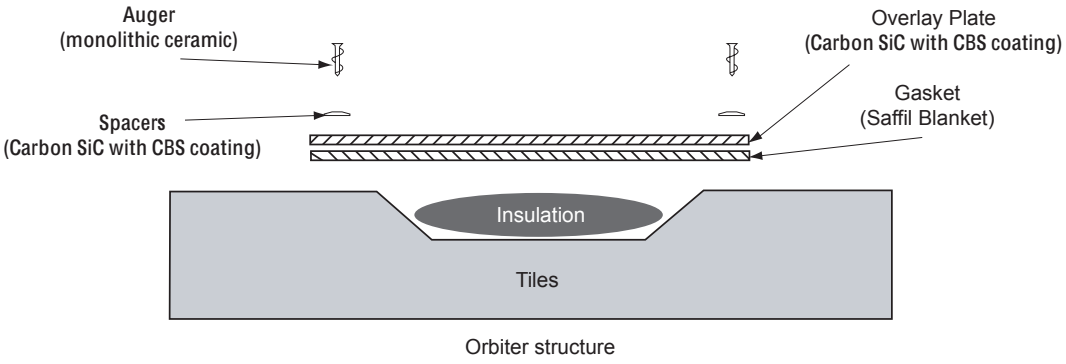

Figure 1. Schematic of the tile overlay including fasteners, gasket, and saffil batting on the damaged shuttle orbiter surface.

In this study, the effects of tile-repair augers on surface heat transfer rate are investigated. To minimize computational time, smooth body Orbiter CFD data is used as a baseline solution. Laminar, five-species gas is assumed, with non-equilibrium, non-ionizing air flow. Thermal radiation is assumed to be at equilibrium on all surfaces with constant emissivity of 0.89.

This report is organized as follows: the nominal surface heat transfer rate on the smooth body shuttle orbiter is given in Section 2. Section 3 presents descriptions of the TOR and physical properties of the augers and spacers used in the analyses. Results of the tile-repair auger analyses are presented in Section 4. Finally, a brief summary of the results is provided in Section 5.

2 Smooth Body Shuttle Orbiter

A shuttle orbiter STS-107 trajectory point is considered with a free-stream velocity $U = 5536.49\ m/s$ [18164.34 ft/s], density $\rho = 0.26069 \times 10^{-3}\ kg/m^3$ [$1.63 \times 10^{-5}\ lb/ft^3$], temperature T =238.48 K [429.26 R], and angle of attack $\alpha = 39.02°$. The corresponding Mach number is $M = 17.85$. Free-stream flow conditions, including the shuttle altitude, are tabulated in Table (1). These flow conditions are essentially the same for both STS and ISS-HVFW trajectories at Mach 17.85 (see Lessard [7]).

Table 1. Free-Stream Flow Conditions.

H	**T**	**U**	**M**	ρ	α
(km)	(K)	$(\frac{m}{s})$	-	$(\frac{kg}{m^3})$	degrees
60	238.48	5536.49	17.85	0.26069×10^{-3}	39.02

In the TOR computational aeroheating analyses, the solution of the smooth body shuttle orbiter is imposed as an initial condition. Due to the hypersonic nature of the flow field surrounding the damaged area, the flow condition upstream of the tile remains unchanged and therefore is not simulated; thus, only a small portion of the shuttle around the damaged site is modeled.

Figure (2) shows the heat transfer rate on the surface of the shuttle orbiter, normalized to the nominal heat transfer rate located at BPt1800 ((x, y, z) = (32.13 m [1265 in], 0, 6.63 m [261 in]), with respect to the orbiter's reference coordinate system). This normalized heat transfer rate is referred to as the *Bump Factor* (BF). Surface heat transfer rate at the damage site is computed as 5.63 W/cm^2 [4.96 $BTU/ft^2.sec$].

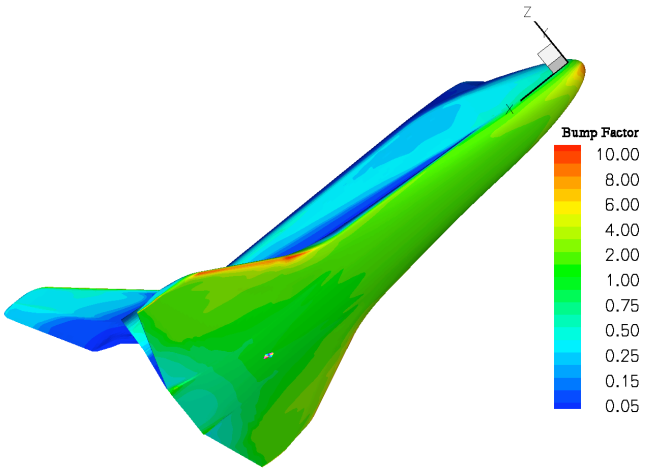

Figure 2. Contour variations of bump factor based on the BPt1800 on the surface of the smooth body shuttle orbiter at $Mach = 17.85$ and $\alpha = 39.02°$.

Note that the boundary layer thickness at BPt1800 is $\delta = 5.13\ cm$ [2.02 in], which is thicker than the tile overlay by a factor of about 20. Therefore, it is less likely that the boundary layer transition occurs at this small k/δ ratio.

3 Tile Overlay Repair

As previously described, the tile overlay, which is an on-orbit patch for thermal protection of the damaged site, is considered for the tile repair aerothermodynamic analysis. In this analysis the overlay plate central bulge that is due primarily to the presence of insulation materials underneath the TOR is not included. The gasket location is schematically shown in Figure (1). The tile overlay is modeled as a protuberance of 38.1 $cm \times 63.5$ cm$\times 0.254$ cm [15 $in \times 25$ $in \times$ 0.1 in] with rounded edges of 8.9 cm [3.5 in] radii. The aerothermodynamic results of the tile overlay will be used as a baseline solution for analysis of the augers and spacers. Discussion of the tile-repair auger analyses are given in subsequent sections.

Figure (3) shows the overlay with structured surface grid used in aeroheating analyses of the tile overlay. The grid is carefully generated near the edges of the overlay to preserve the viscous boundary layer. Using the orbiter *Atlantis* tile layout, the overlay is parallel to the tile edges, which lie at a 45° angle with respect to the orbiter centerline. A schematic of the damaged site, orientation of the tile overlay repair, and location of BPt1800 are shown in Figure (4).

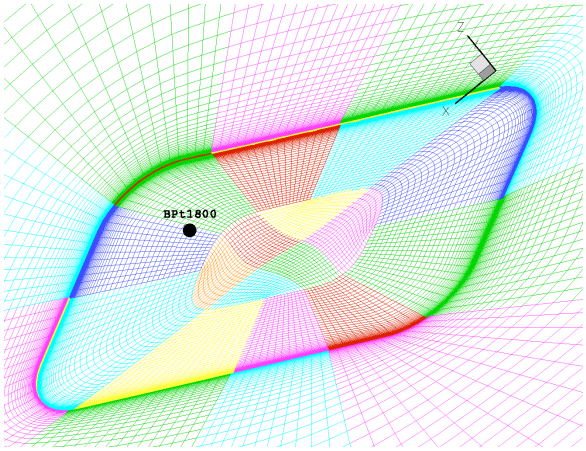

Figure 3. The tile overlay with the surface grid, and the reference point BPt1800.

3.1 Tile Overlay Fasteners *(Spacers & Augers)*

Several augers are used to patch the tile overlay repair to the shuttle surface. Due to the high conductivity of these augers and spacers, heat may conduct to the layer underneath the tiles, leading to a significant increase in temperature of the tile bond line and aluminum substructure of the orbiter.

In this study, spacers are approximated as protuberances with diameter $d = 2.16$ cm [0.85 $inch$] and height of $h = 0.14$ cm [0.055 in]. (The auger head is a circle with diameter $d_{auger} = 1.37$ cm [0.54 in] in the center of the spacer cylinder. The top of the auger head and the spacer head are on the same surface.)

4 Entry Aeroheating Computations

Entry aeroheating computations are performed to investigate the effects of tile overlay protuberance on surface heat transfer rate. The Langley Aerothermodynamic Upwind Relaxation Algorithm (LAURA) [3,4] was employed for the entire study. LAURA is a hypersonic,

multi-species, chemical reacting code developed for re-entry arothermodynamic analyses. In this study, a non-equilibrium, non-ionizing, five-species air model is considered under the laminar flow condition. Non-equilibrium processes occur when the time required for a process to accommodate itself to local conditions within a region is of the same order as the transit time within the same region. Since the particle time relaxation-pressure correlation is not precisely known, and there is no evidence that at this flow condition gas is at thermal non-equilibrium [5], thermal equilibrium is assumed. Note that ionization does not occur until the temperature reaches $9000K$. Based on the trajectory point considered here, and according to the velocity-altitude map reported by Anderson [1] and Koppenwallner [6], the air is not ionized at this point.

Radiative equilibrium wall temperature with constant emissivity of $\epsilon = 0.89$ and Reaction Cured Glass (RCG) catalycity are assumed. Note that engineering approximations can be made for different emissivity and catalycity conditions by multiplying the emissivity ratio with the normalized heat transfer rate, or bump factor. Hence, higher emissivity leads to higher heat fluxes.

Again, the computational result of the smooth body shuttle orbiter is used as an initial condition. The computational domain considered to study the effects of protuberances on aeroheating is about five times larger than the tile overlay surface area. This relatively small computational domain is chosen because any flow disturbance due to overlay and/or augers rapidly diffuses within the viscous region.

Only spacers and augers thought to be the most critical are analyzed. The augers are chosen according to predicted surface heat transfer rate on the overlay protuberance. Results for these critical spacers and augers will be used in future structural thermal analyses and tile overlay failure assessment studies.

4.1 Tile Overlay Aerothermodynamic Analysis

The tile overlay placed on the damage site is shown schematically in Figure (4). This overlay alignment is referred to as *Overlay Placement number 3*. The tile overlay is discretized using a multi-block structured grid with dimensions $(i, j, k) = (16, 74, 64)$. Figure (3) shows the tile overlay surface grid. The computational domain with appropriate boundary conditions is shown in Figure (5).

The computations were performed for a free-stream Mach number $M = 17.85$ and Temperature $T = 238.48$ K [429.26 R], at 39.02° angle of attack α. Convergence was achieved after nearly 20,000 iterations and until no further significant changes were observed. Figure (6) shows Mach contour variations at a section perpendicular to the tile overlay. This figure shows that the flow field remained supersonic, which further verifies the assumptions made.

Variations of tile overlay surface temperature are shown in Figure (7). Note that flow is in the positive x direction. Figure (7) shows a jump in surface temperature at the upstream edge of the overlay. This jump is due to the high kinetic energy of the gas, and the fact that the overlay edges are modeled as sharp rather than rounded edges.

The surface heat transfer rate distribution, normalized with respect to BPt1800, is shown in Figure (8). This figure shows approximately 2.5 times higher heat transfer rate on the upstream edge of the overlay when compared with BPt1800. A relatively uniform surface heat transfer rate is predicted for the rest of the overlay with slightly higher values than BPt1800.

The result of a more detailed analysis of overlay surface BF variation is shown in Figure (9). Figure (9a) shows tile surface BF variation, with distance measured from the most upstream corner and along the flow direction. The surface heat transfer rate decreases

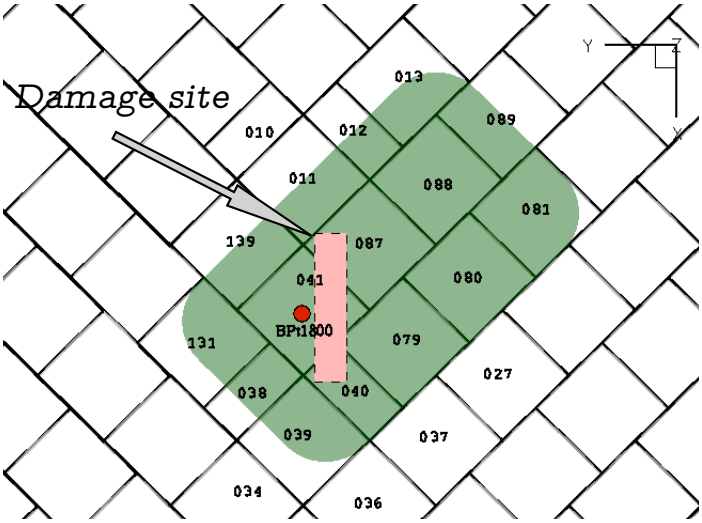

Figure 4. Schematic of the CFD tile overlay repair and its location with the *Atlantis* tile layout on the damage site. (View from outside of the Orbiter, with its nose toward top of the page.)

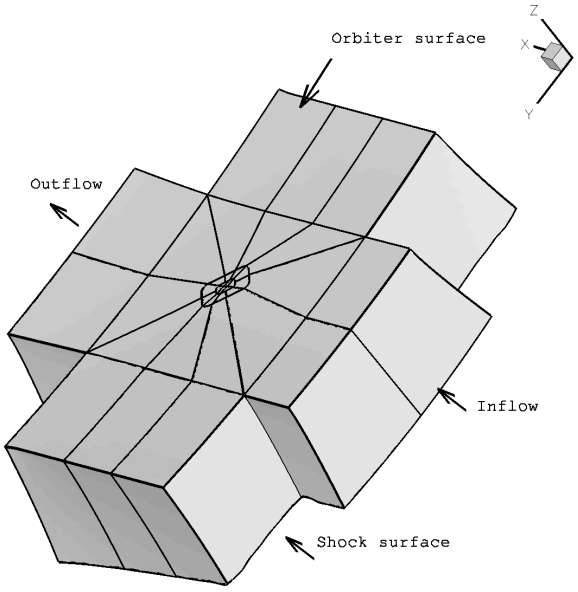

Figure 5. Schematic of the computational domain and boundary conditions used for aerothermodynamic analysis of the tile overlay. (The view is looking from the inside of the Orbiter structure out into the flowfield.)

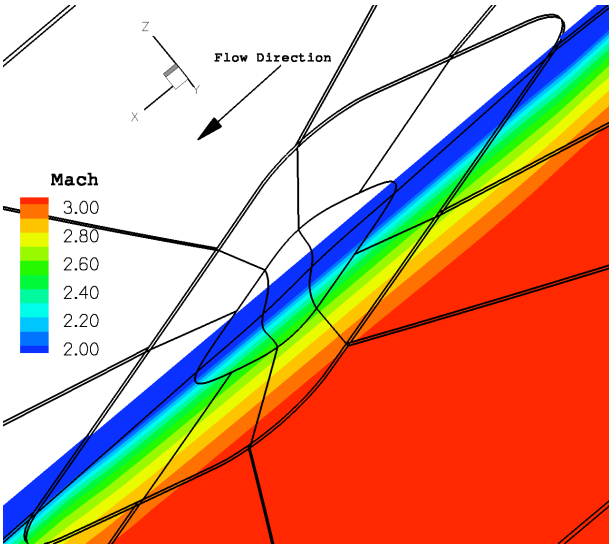

Figure 6. Mach contour variations at a section perpendicular to the tile overlay surface at Mach number $M = 17.85$ and $\alpha = 39.02°$.

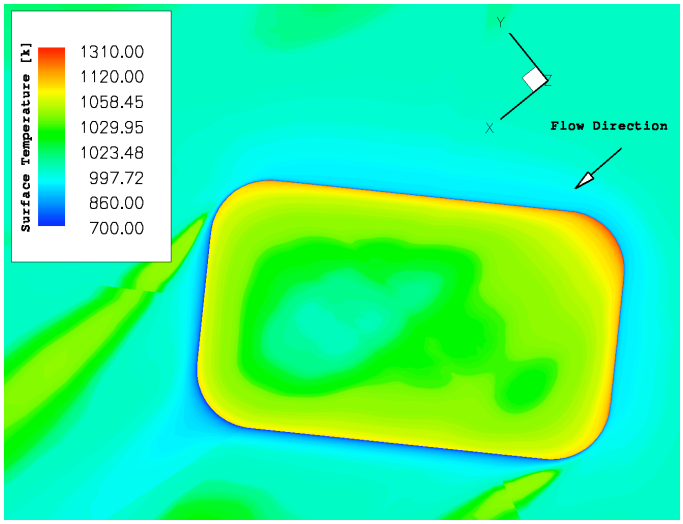

Figure 7. Tile overlay surface temperature variations at Mach number $M = 17.85$ and $\alpha = 39.02°$.

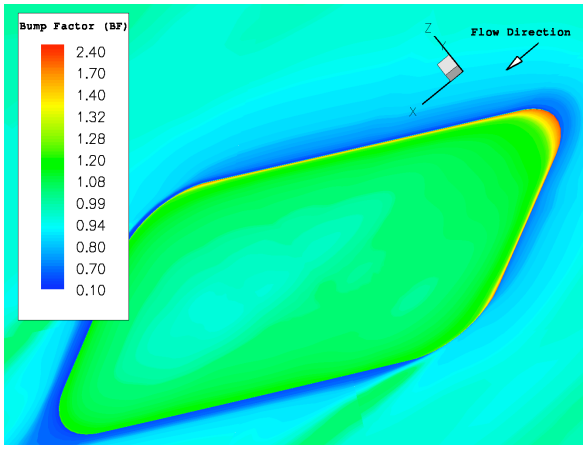

Figure 8. Variations of bump factor with respect to Body Point 1800 (BPt1800) on the surface of the tile overlay at $M = 17.85$ and $\alpha = 39.02°$.

sharply from BF=2.4 to about BF=1.2 as flow moves away from the tile overlay corner. An inset of the figure shows the surface bump factor variation near the upstream TOR edge. This close-up figure shows a minimum BF of about 1.0 at a distance of about 10 *inches* from the upstream TOR edge.

Figure (9b) shows the tile overlay surface bump factor, normalized with respect to BPt1800, across the overlay width as shown with the arrow. Figure (9b) shows that the BF decreases quickly from about 1.5 at the tile edge to about 1.0 on downstream of the tile edge. The BF continues to decrease until the flow reaches approximately 80% of the tile's width. The BF then increases to 1.20 at the other side of the tile overlay.

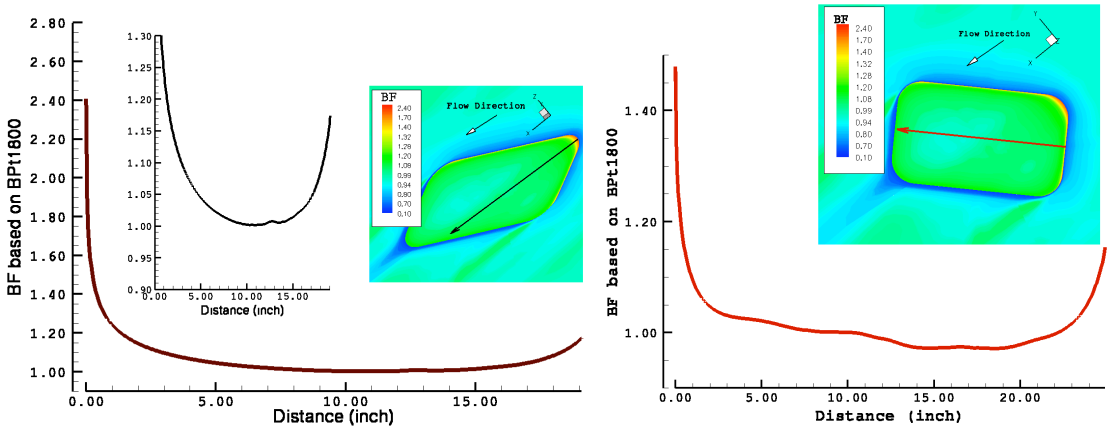

Figure 9. Variations of the tile overlay surface bump factor with a) distance from the upstream corner of the overlay along the flow direction, and b) distance across the tile overlay.

4.2 Augers & Spacers Aeroheating Analysis

According to aeroheating analyses of the tile overlay, shown in Figures (7)-(9), the augers located on the upstream edge of the overlay are critical to the aerothermal analysis. Therefore, these augers are considered for areohermodynamic analyses. The spacers and augers are approximated as protuberances with heights of 0.14 cm [0.0552 in] and diameters of d = 2.16 cm [0.85 in]. (Note again that the auger head is in the central region of the spacer with a diameter of d_{auger} = 1.37 cm [0.54 in].) The center of the first auger considered here is located at (x, y, z) = (31.75 m, 0.24 m, 6.61 m)[1250.58 in, -9.48 in, 260.44 in]. Figure (10) shows schematically the location of this auger on the tile overlay.

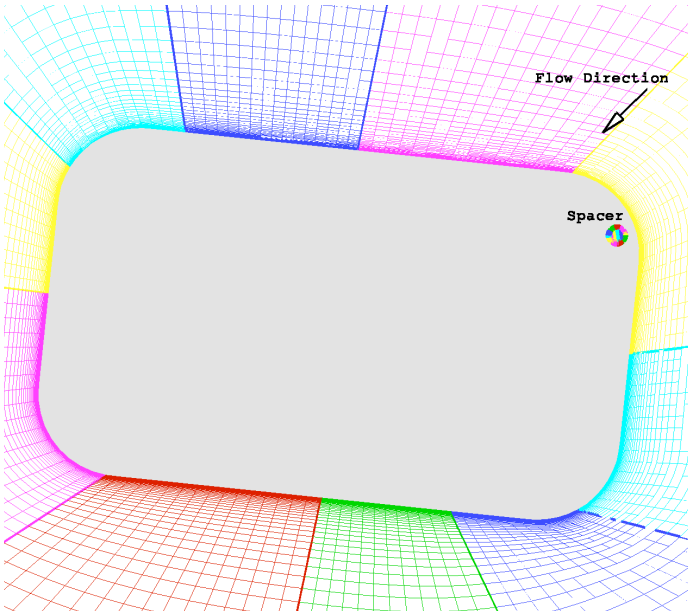

Figure 10. Schematic of the location of the auger/spacer on the tile overlay.

Parametric studies were conducted for grid sensitivity analyses. Computational grids with four different resolutions were generated as shown in Figure (11). Computational entry aeroheating analyses were performed for all four cases to determine auger surface heat transfer rate distributions. Figure (12) shows heat transfer rate variation on the auger surface. Flow is in the positive x direction. Figure (12) shows that the surface heat transfer predictions are in good agreement for all cases.

To better examine the aeroheating results, surface heat transfer rates were normalized with respect to BPt1800. Figure (13) shows BF contour variation on auger, spacer, and overlay surfaces. This figure shows that the computed results are insensitive to grid resolutions. Figure (13) shows a BF of about 3.0 at the edges of the spacer. The actual spacer geometry is approximated as a protuberance with sharp edges as opposed to rounded edges. Thus, the edge BF may not reflect an actual value.

A more detailed surface BF distribution on auger and spacer heads is shown in Figure (14). This figure shows variations of the surface BF with two distances; one from the upstream edge of the spacer along the flow direction (shown with longer arrow) and the other perpendicular to the flow direction and across the spacer (shown with shorter arrow). The distance between the edges of the overlay and the spacer is marked *upstream* with negative values on the x axis. The second part of the graph belongs to the auger and spacer

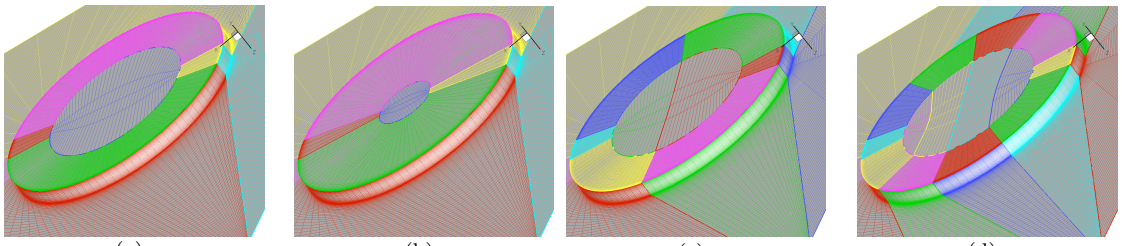

(a) (b) (c) (d)

Figure 11. Computational grids for the auger and spacer with different resolutions; a) four blocks for the spacer surface and one block for the auger surface, b) five blocks for both spacer and auger surfaces, c)six blocks for spacer surface and two grid blocks for auger surface, d)ten blocks for the spacer surface and four grid blocks for the auger surface.

heads. Part of the graph that corresponds to the auger head is also marked for clarification. Figure (14) shows the BF decreases from 2.4 at the upstream edge of the overlay to about 0.5 just upstream of the spacer edge. As the gas flow sees an immediate increase in surface height, the surface heat transfer jumps to a maximum value of BF=3.9 at the edge of the spacer. The BF then dissipates as the flow moves toward the other side of the spacer.

The spacer surface BF on a plane perpendicular to the flow direction is shown in Figure (14). BF variation is shown with a dark line in this figure, which shows a relatively uniform surface heat flux with nominal value of about BF=2.0.

To estimate the overall BF on the surfaces of the auger and spacer, BF values are integrated over the surface area. These results are tabulated in Table (2), which shows an overall BF of about 2 for auger and spacer surfaces. The numerical results were almost exactly the same for all different grid resolutions.

Table 2. Normalized heat transfer rate, BF, for auger and spacer surfaces with different grid resolutions.

		Bump Factor (BF) with respect to BPt1800	
		Auger Surface	Auger + Spacer Surfaces
Grid Resolution	a	1.91	2.02
	b	1.93	2.02
	c	1.93	2.02
	d	1.91	2.02

4.2.1 Spacer Aeroheating Analysis (with larger computational domain)

To assure that such a small computational domain was sufficient in the aeroheating analysis, a larger computational domain was considered and compared with previous results. Figure (15) shows a multi-block surface grid for this larger domain. In this case, grid resolution (b) was adapted for the spacer and auger. A total of 119 blocks was generated for this case.

Flow conditions with identical thermodynamic properties were employed. Figure (16) shows the computed aeroheating results of normalized surface heat transfer rate, BF, for the spacer, auger, and tile overlay. Figure (16a) shows the corresponding BF contour variations

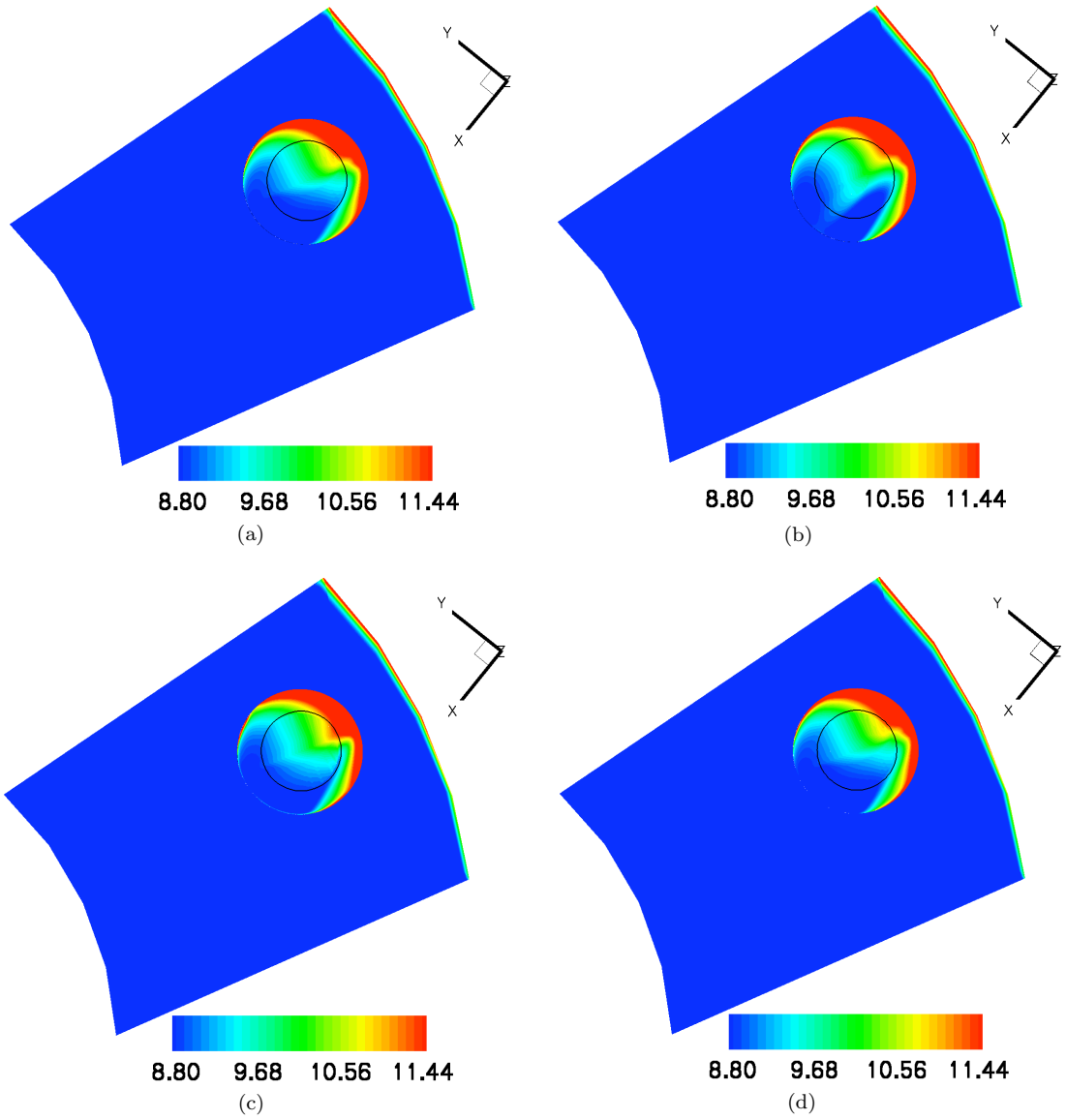

Figure 12. Contour variations of heat transfer rate $[\frac{BTU}{ft^2.sec}]$ with grid resolution (a), (b), (c), and (d). flow conditions are at $M = 17.85$ and $\alpha = 39.02°$.

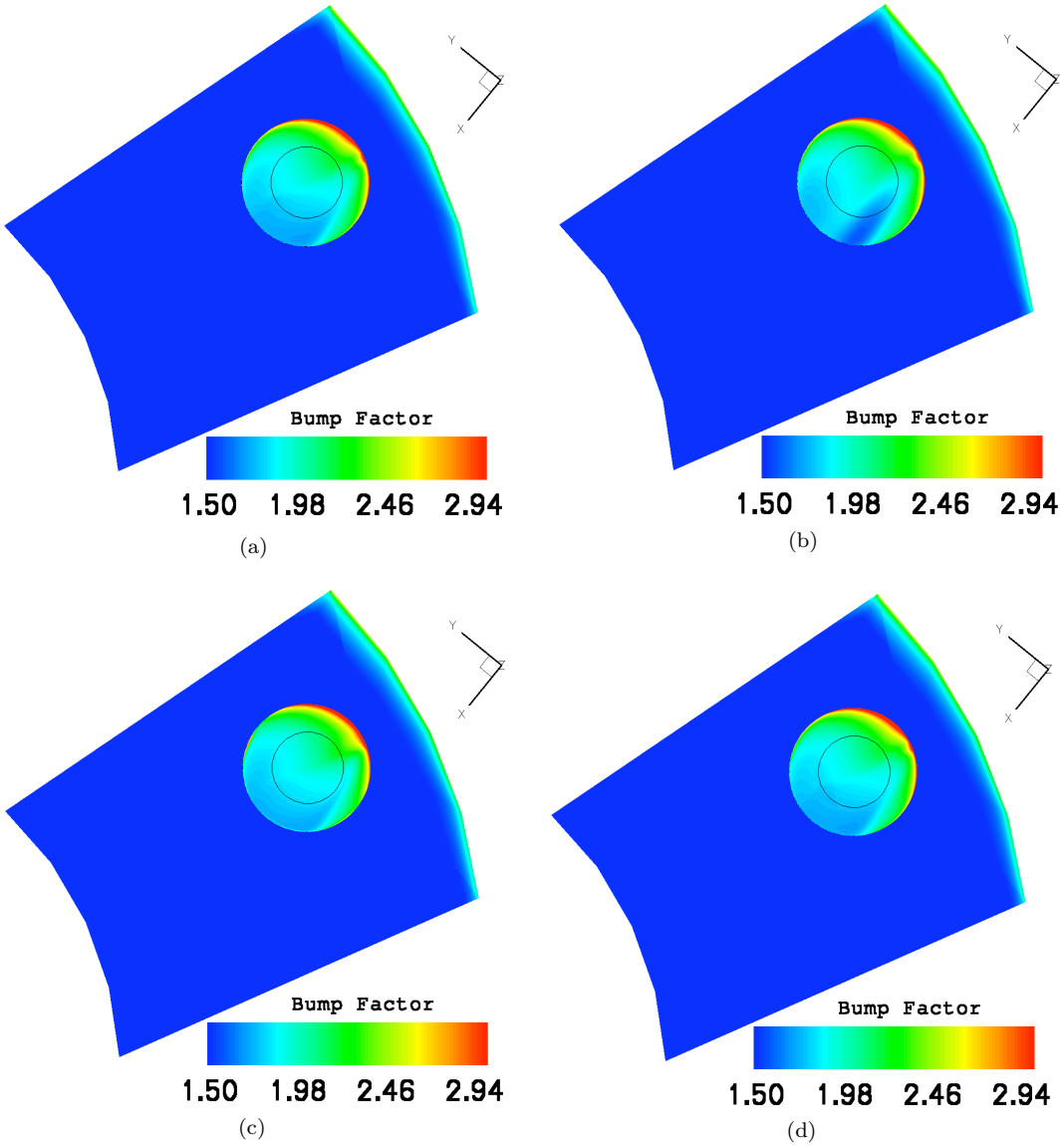

Figure 13. Contour variations of normalized surface heat transfer rate (*Bump Factor*) with grid resolution (a), (b), (c), and (d). Flow conditions are at $M = 17.85$ and $\alpha = 39.02°$.

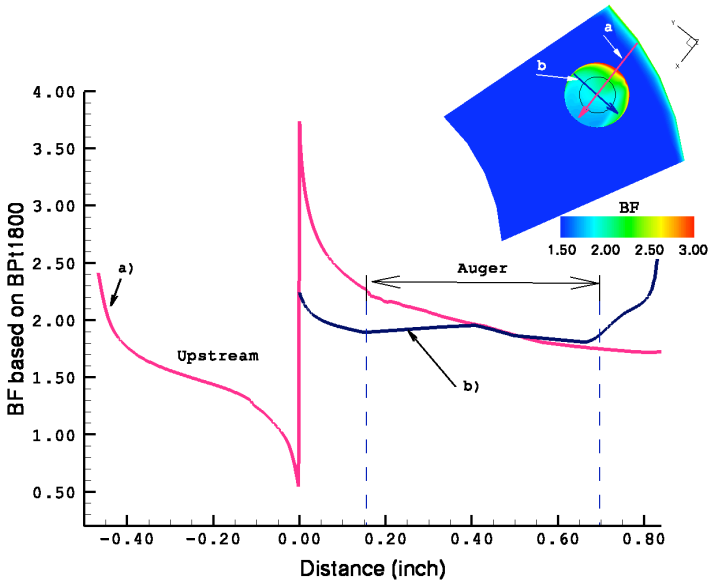

Figure 14. Variations of the auger and spacer surfaces bump factor with distances a) from the upstream edge of the tile overlay, along the direction, and b) across the spacer and auger, perpendicular to the flow direction.

and a very high surface heat flux with BF of about 3.3 on the upstream edge of the spacer. This high BF was primarily due to the fact that the spacer was modeled as a protuberance with sharp edges. Variations of the auger/spacer surface BF with distance are shown in Figure (16b). The distance is measured from the upstream edge of the spacer and along the flow direction. Figure (16b) shows a maximum BF of about 3.3 at the most upstream corner of the spacer. This BF then decreases to a minimum value of about BF=2.0 on the most downstream location of the spacer. The surface BF on the tile overlay repair downstream of the spacer and along the flow direction is shown in Figure (16c). This figure shows a low BF of about 0.4 just downstream of the spacer. This value increases quickly to about BF=1.2 afterward, and monotonically increases to a maximum of about BF=1.6 on the downstream edge of the tile.

In order to compare the results, average surface bump factors on the spacer and auger surfaces were evaluated. The average surface BF for the combined auger and spacer surfaces was about 2.05, in close agreement with that reported in Table (2) using a smaller computational domain. This justified the small-domain consideration in aeroheating analysis. Note, however, that computational aerothermodynamic analyses of the spacer and auger on the tile overlay using a larger domain provided a more in-depth understanding of the tile overlay surface heat fluxes.

4.3 Tandem Auger & Spacer Aeroheating Analysis

Effects of tandem auger and spacer on the aeroheating were investigated. Location of the tandem auger is schematically shown in Figure (17). In this case, grid resolution (a) of Figure (11) was adapted for each one of the augers and spacers. Both spacers were included in the aeroheating calculations; the single spacer solution was not reused during this analysis to allow for possible interference effects.

Computational aeroheating analysis was performed and surface heat transfer rate and

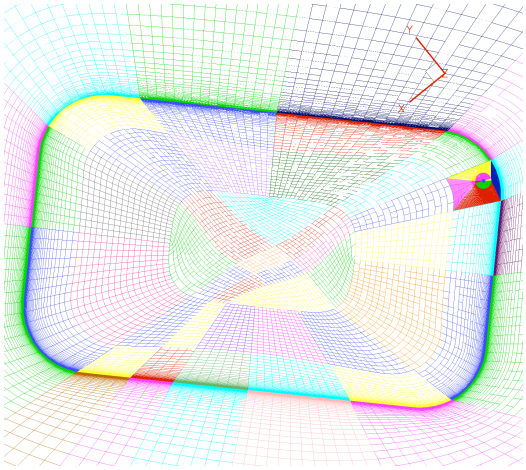

Figure 15. Surface grid used for the spacer seroheating analysis using larger computational domain.

bump factor were calculated. Figure (18) shows variations of heat transfer rate for the tandem. It is seen from this figure that only a small portion of the tandem surface is exposed to high temperature gas flow. Based on the computational studies, no significant effects of upstream spacer on downstream spacer surface heat transfer rate was observed. Also, flow-channeling did not occur between these spacers. There is, however, a possibility that the flow regime may be transient and/or turbulent downstream of the spacers. This possibility is not considered here.

Figure (19) shows the surface bump factor, BF, for the tandem auger. Similar to the graph shown in Figure (14), a line-cut through downstream spacer and auger is shown in this figure for comparison. This figure shows that the normalized auger surface heat transfer rate remains unchanged with BF of about 1.91. However, the upstream spacer surface BF is increased with the combined auger and spacer BF of 2.07. Note that based on the aeroheating results of the individual auger and spacer on the tile overlay, BF is 2.02. Figure (19) shows a decrease in surface BF from the leading edge of the tile overlay and a sudden increase in its value at the upstream edge of the spacer to a maximum value of about BF=3.0. This high surface heat transfer rate drops quickly and reaches a minimum value of BF=1.6 downstream of the spacer. These results are tabulated in Table (3). This table indicates that the downstream auger surface BF is 1.77, which is less than that for the upstream one. The combined auger and spacer BF for the downstream one is, however, 1.91. A comparison was made with the previous study where only the upstream auger was modeled. Table (3) shows that the auger BF located on the most upstream edge of the tile overlay is not affected by the downstream auger.

Table 3. Tabulated data of normalized heat transfer rate, BF, for auger and spacer surfaces for different modeling types.

Modeling Type		**Bump Factor (BF) with respect to BPt1800**	
		Auger Surface	Auger + Spacer Surfaces
Tandem	Upstream	1.91	2.07
	Downstream	1.77	1.91
Individual (from Table 2)		1.91	2.02

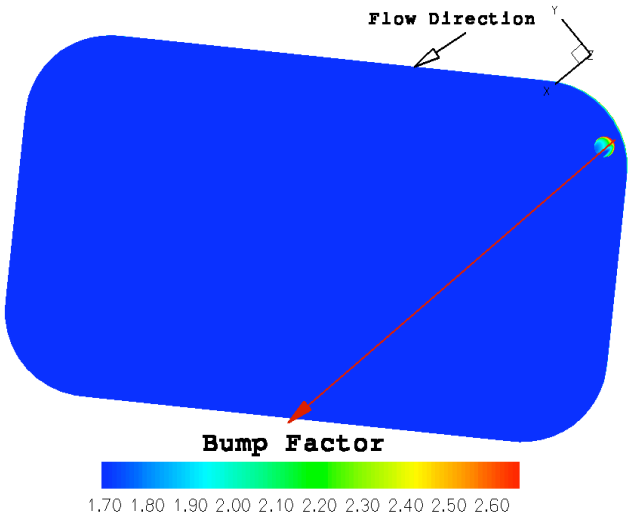

(a)

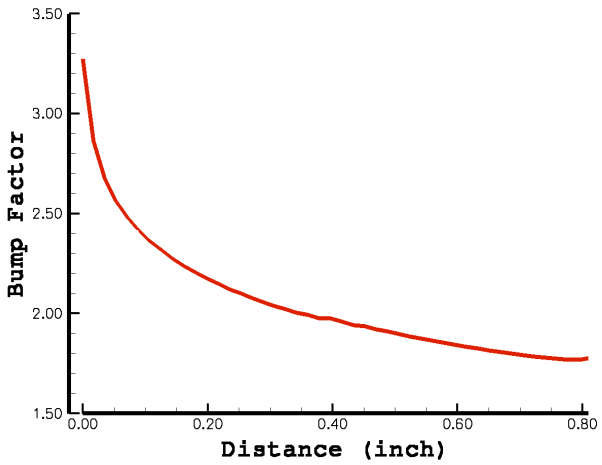

(b)

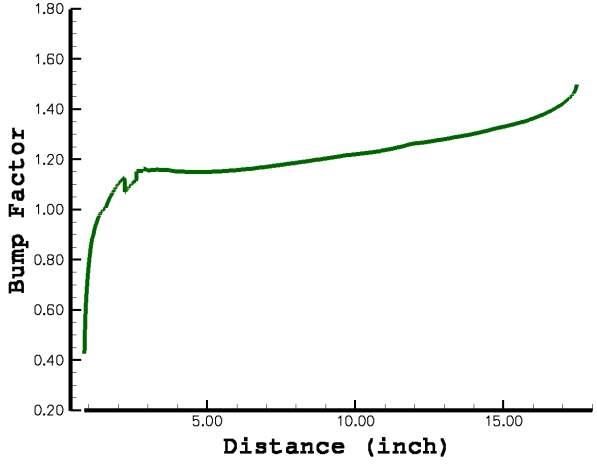

(c)

Figure 16. a)Surface bump factor, BF, variations computed bases on the BPt1800 on the surface of the overlay and spacer using the grid shown in Figure(15); b)Bump factor variations on the surfaces of the auger and spacer with distance from the leading edge of the spacer along the flow direction; and c)Bump factor variations on the surface of the tile overlay downstream of the spacer with distance along the flow direction.

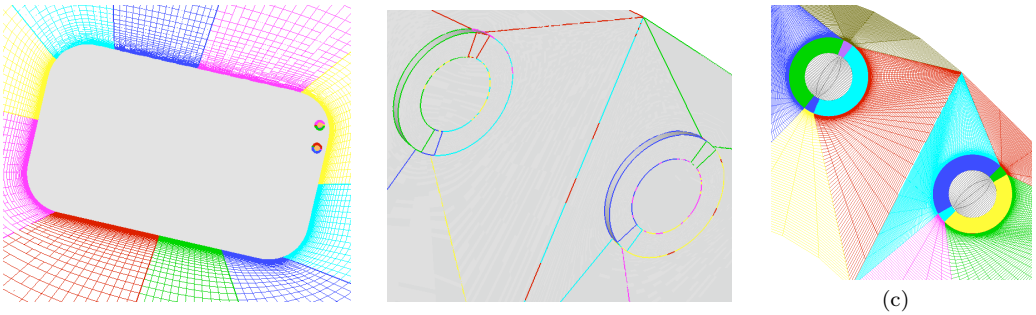

(a) (b) (c)

Figure 17. Location of the tandem auger and spacer on the tile overlay, b) geometries and boundaries of the tandem auger and spacer, and c) the tandem multi-block structured grids.

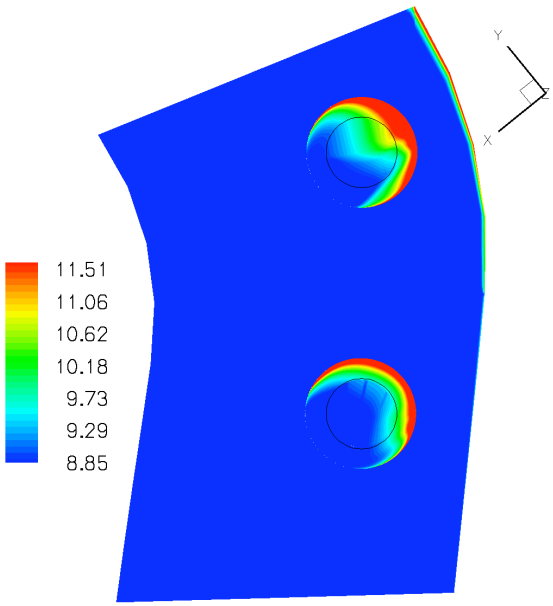

Figure 18. Variations of the tandem auger and spacer surfaces heat transfer rate $[\frac{BTU}{ft^2.sec}]$ with flow conditions at $M = 17.85$ and $\alpha = 39.02°$.

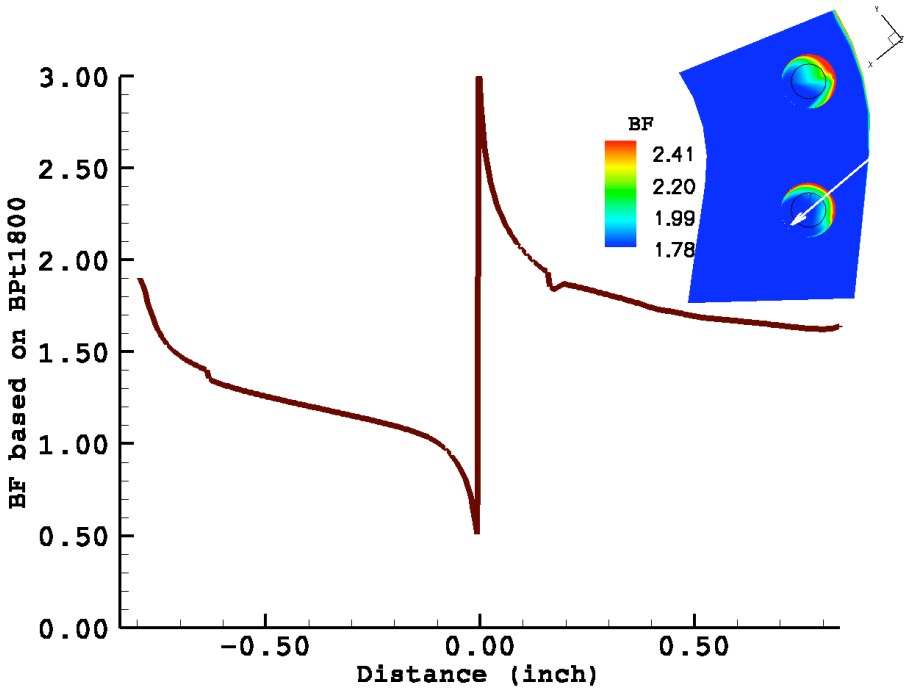

Figure 19. Variations of the normalized surface heat transfer rate, BF, for the tandem auger and spacer surfaces with flow conditions at $M = 17.85$ and $\alpha = 39.02°$.

5 Conclusions

In this investigation shuttle orbiter return to flight entry aeroheating analyses were conducted. Aerothermodynamic properties of a specific Tile Overlay Repair, including fasteners (spacers and augers), were numerically analyzed using the Langley Aerothermodynamics Upwind Relaxation Algorithm (LAURA) for a Mach 17.85 trajectory point. Non-equilibrium, non-ionizing five species gas was assumed, and the surface temperature and heat transfer rate distributions were computed. On the basis of the presented results, the following conclusions may be drawn:

- The upstream edge of the Tile Overlay Repair is exposed to the highest gas temperature of about $1300K$ at the Mach 17.85 trajectory point, and a heat transfer rate equivalent to Bump Factor of about 2.4.

- The aeroheating analyses are insensitive to grid resolutions studied in this investigation.

- In modeling the individual auger on the tile overlay, the average normalized surface heat transfer rate with respect to BPt1800 is BF=1.9. The combined auger and spacer BF is 2.02, however.

- In analysis of the tandem auger, the upstream spacer did not significantly affect the aeroheating properties of the downstream auger. The average downstream auger surface BF is 1.77, while the combined auger and spacer surface BF is 1.91.

Acknowledgment

The author would like to thank Dr. William A. Wood of NASA Langley Research Center for many helpful discussions. Thanks are also given to Victor Lessard, from Genex Systems, Dr. Sasan Armand, Pawel Chwalowski, and John Van Norman, from AMA Inc., for their technical supports and reviewing the report. This work was performed under the contract number NNL06AC49T.

References

1. Anderson, J.D., High-Temperature Gas Dynamics, McGraw-Hill Book Co., 1985.

2. Campbell, C.H., Anderson, B., Bourland, G., Bouslog, S., Cassady, A., Horvath, T.J., Berry, S.A., Gnoffo, P.A., Wood, W.A., Reuther, J.J., Driver, D.M., Chao, D.C., Hyatt, J., and Picetti, D., "Orbiter Return to Flight Aeroheating", 9^{th} AIAA/ASME Joint Thermophysics and Heat Transfer Conference, San Francisco, CA, June 5-8, 2006.

3. Gnoffo, P.A., "An Upwind-Biased, Point-Implicit Relaxation Algorithm for Viscous, Compressible Perfect-Gas Flows", NASA TP2953, February 1990.

4. Gnoffo, P.A., Gupta, R.N., and Shinn, J.L., "Conservation Equations and Physical Models for Hypersonic Air Flows in Thermal and Chemical Nonequilibrium", NASA TP2867, February 1989.

5. Gnoffo, P.A., Private conversation with the author, September 2006.

6. Koppenwallner, G., "Fundamentals of Hypersonics: Aerodynamics and Heat Transfer", in the short course entitled *Hypersonic Aerothermodynamics*, presented at the Von Karman Institute for Fluid Dynamics, Rhose Saint Genese, Belgium, February 1984.

7. Lessard, V.R., "CFD-Predicted Tile Heating Bump Factors Due to Tile Overlay Repairs", NASA Langley Research Center, NASA CR2006-214509, 2006.

REPORT DOCUMENTATION PAGE

Form Approved
OMB No. 0704-0188

1. REPORT DATE *(DD-MM-YYYY)*	2. REPORT TYPE	3. DATES COVERED *(From - To)*
01- 04 - 2007	Contractor Report	

4. TITLE AND SUBTITLE

CFD Analysis of Tile-Repair Augers for the Shuttle Orbiter Re-Entry Aeroheating

5a. CONTRACT NUMBER

5b. GRANT NUMBER

NNL06AC49T

5c. PROGRAM ELEMENT NUMBER

6. AUTHOR(S)

Mazaheri, Ali R.

5d. PROJECT NUMBER

5e. TASK NUMBER

5f. WORK UNIT NUMBER

7. PERFORMING ORGANIZATION NAME(S) AND ADDRESS(ES)

NASA Langley Research Center
Hampton, VA 23681-2199

Analytical Mechanics Associates, Inc.
Hampton, VA 23666

8. PERFORMING ORGANIZATION REPORT NUMBER

9. SPONSORING/MONITORING AGENCY NAME(S) AND ADDRESS(ES)

National Aeronautics and Space Administration
Washington, DC 20546-0001

10. SPONSOR/MONITOR'S ACRONYM(S)

NASA

11. SPONSOR/MONITOR'S REPORT NUMBER(S)

NASA/CR-2007-214858

12. DISTRIBUTION/AVAILABILITY STATEMENT

Unclassified - Unlimited
Subject Category 64
Availability: NASA CASI (301) 621-0390

13. SUPPLEMENTARY NOTES

Langley Technical Monitor: William A. Wood
An electronic version can be found at http://ntrs.nasa.gov

14. ABSTRACT

A three-dimensional aerothermodynamic model of the shuttle orbiter's tile overlay repair (TOR) sub-assembly is presented. This sub-assembly, which is an overlay that covers the damaged tiles, is modeled as a protuberance with a constant thickness. The washers and augers that serve as the overlay fasteners are modeled as cylindrical protuberances with constant thicknesses. Entry aerothermodynamic cases are studied to provide necessary inputs for future thermal analyses and to support the space-shuttle return-to-flight effort. The NASA Langley Aerothermodynamic Upwind Relaxation Algorithm (LAURA) is used to calculate heat transfer rate on the surfaces of the tile overlay repair and augers. Gas flow is modeled as non-equilibrium, five species air in thermal equilibrium. Heat transfer rate and surface temperatures are analyzed and studied for a shuttle orbiter trajectory point at Mach 17.85. Computational results show that the average heat transfer rate normalized with respect to its value at body point 1800 is about BF=1.9 for the auger head. It is also shown that the average BF for the auger and washer heads is about BF=2.0.

15. SUBJECT TERMS

Re-entry Aeothermodynamics; CFD; Tile Overlay; Shuttle Orbiter

16. SECURITY CLASSIFICATION OF:			17. LIMITATION OF ABSTRACT	18. NUMBER OF PAGES	19a. NAME OF RESPONSIBLE PERSON
a. REPORT	b. ABSTRACT	c. THIS PAGE			STI Help Desk (email: help@sti.nasa.gov)
U	U	U	UU	23	19b. TELEPHONE NUMBER *(Include area code)* (301) 621-0390